Spectra of CO_2-Rg_2 and CO_2-Rg-He trimers (Rg = Ne, Ar, Kr, and Xe): Intermolecular CO_2 rock, vibrational shifts and three-body effects

Barclay, A. J.; McKellar, A. R. W.; Moazzen-Ahmadi, N.

Publisher's version / Version de l'éditeur:
https://doi.org/10.1063/5.0128133
The Journal of Chemical Physics, 157, 20, 2022-11-22

The Journal of Chemical Physics ARTICLE scitation.org/journal/jcp

Spectra of CO_2-Rg_2 and CO_2-Rg-He trimers (Rg = Ne, Ar, Kr, and Xe): Intermolecular CO_2 rock, vibrational shifts and three-body effects

Cite as: J. Chem. Phys. 157, 204303 (2022); doi: 10.1063/5.0128133
Submitted: 26 September 2022 • Accepted: 31 October 2022 •
Published Online: 22 November 2022

A. J. Barclay,[1] A. R. W. McKellar,[2] and N. Moazzen-Ahmadi[1,a)]

AFFILIATIONS

[1] Department of Physics and Astronomy, University of Calgary, 2500 University Drive North West, Calgary, Alberta T2N 1N4, Canada
[2] National Research Council of Canada, Ottawa, Ontario K1A 0R6, Canada

[a)] **Author to whom correspondence should be addressed:** nmoazzen@ucalgary.ca

ABSTRACT

Weakly bound CO_2-Rg_2 trimers are studied by high-resolution (0.002 cm^{-1}) infrared spectroscopy in the region of the CO_2 ν_3 fundamental band (≈2350 cm^{-1}), using a tunable optical parametric oscillator to probe a pulsed supersonic slit jet expansion with an effective rotational temperature of about 2 K. CO_2–Ar_2 spectra have been reported previously, but they are extended here to include Rg = Ne, Kr, and Xe as well as new combination and hot bands. For Kr and Xe, a unified scaled parameter scheme is used to account for the many possible isotopic species. Vibrational shifts of CO_2-Rg_2 trimers are compared to those of CO_2-Rg dimers, and in all cases the trimer shifts are slightly more positive (blue-shifted) than expected on the basis of linear extrapolation from the dimer. Combination bands directly measure an intermolecular vibrational mode (the CO_2 rock) and give values of about 32.2, 33.8, and 34.7 cm^{-1} for CO_2–Ar_2, –Kr_2, and –Xe_2. Structural parameters derived for CO_2-Rg_2 trimers are compared with those of CO_2-Rg and Rg_2 dimers. Spectra of the mixed trimers CO_2-Rg-He are also reported.

I. INTRODUCTION

Thanks to their fundamental nature and experimental accessibility, CO_2–rare gas (Rg) clusters serve as useful probes of intermolecular force effects to help improve theoretical modeling. The CO_2-Rg dimers have been extensively studied by high-resolution spectroscopy, beginning with the 1979 work of Steed *et al.*[1] on pure rotational transitions of CO_2–Ar. Some key experimental spectroscopic results in the microwave and infrared regions can be found in Refs. 2–4 for CO_2–He, Refs. 5–9 for CO_2–Ne, Refs. 1, 5, 6, and 10–15 for CO_2–Ar, Refs. 5, 6, and 16–18 for CO_2–Kr, and Refs. 5, 8, 16, and 19 for CO_2–Xe. The equilibrium dimer structures were found to be T-shaped, with the Rg atom located to the "side" of the CO_2, adjacent to the C atom. Effective intermolecular distances (C-Rg) ranged from 3.3 Å for CO_2–Ne to 3.8 Å for CO_2–Xe.

In a notable 1993 paper, Xu *et al.*[20] observed microwave transitions of the trimer CO_2–Ar_2, and this was followed up with infrared observations of CO_2–Ar_2 by Sperhac *et al.*[21] in 1996. As illustrated in Fig. 1, the trimer structure places the second Ar atom in a "side" position equivalent to that of the first, with an Ar–Ar distance of about 3.8 Å, similar to that in the isolated Ar_2 dimer. The trimer is thus an asymmetric rotor with C_{2v} point group symmetry, as is CO_2–Ar. Analogous trimer structures and infrared spectra have also been observed for CO_2–He_2,[22] N_2O–Ar_2, and N_2O–Ne_2.[23] Other weakly bound trimers containing a linear molecule plus two rare gas atoms have also been studied, including OCS-Ar_2,[24] OCS-Ne_2,[25] HCN-Ar_2,[26] and HBr-Ar_2.[27]

In the present paper, we extend the study of CO_2-Rg_2 to include Ne, Kr, and Xe by observing infrared spectra in the region of the ν_3 fundamental band of CO_2 (≈2350 cm^{-1}), the same as for CO_2–Ar_2 in Ref. 21. We also observe combination bands for Ar, Kr, and Xe in addition to the fundamental band. These combinations involve low-frequency (≈30 cm^{-1}) intermolecular modes and thus give new and direct information on trimer vibrational dynamics.

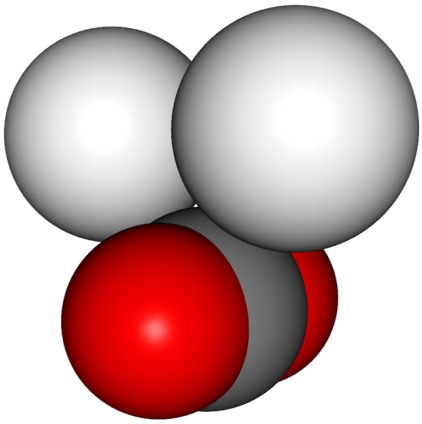

FIG. 1. Illustration of the CO_2-Rg_2 trimer structure. The two Rg atoms at the top in this picture occupy equivalent positions on the equatorial plane of the CO_2 molecule. The twofold rotational symmetry axis (vertical in this picture) is the *a*-inertial axis for Rg = He and Ne, and it is the *b* axis for Rg = Ar, Kr, and Xe.

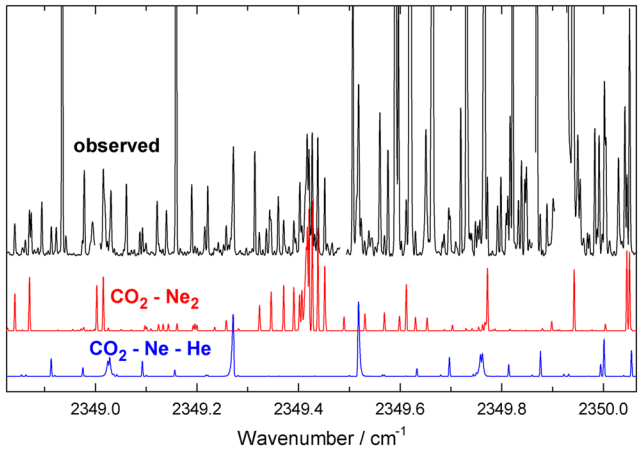

FIG. 2. Observed and simulated spectra showing CO_2–Ne_2 and CO_2–Ne–He in the region of the CO_2 ν_3 fundamental band. The simulation shows only the CO_2–$^{20}Ne_2$ contribution, but transitions of CO_2–^{20}Ne–^{22}Ne were also assigned.

In addition, we observe (limited) trimer spectra corresponding to the CO_2 (ν_1, ν_2^{l2}, ν_3) = (01^11)–(01^10) hot band transition (≈2337 cm^{-1}). All the spectra are recorded using supersonic expansion gas mixtures with helium as the main component, and we are able to observe spectra of the mixed trimers CO_2-Rg-He (Rg = Ne, Ar, Kr, and Xe). As mentioned, CO_2-Rg dimers and CO_2-Rg_2 trimers possess C_{2v} symmetry. For the dimers, where the a-inertial axis is the C_2 symmetry axis, nuclear spin statistics dictate that only levels with (K_a) = (even) are allowed in the ground vibrational state (for $^{12}C^{16}O_2$). The same is true for CO_2–Ne_2, but for CO_2–Ar_2, it turns out that *b* is the symmetry axis, so only levels with (K_a, K_c) = (even, even) or (odd, odd) are allowed. For CO_2–Kr_2 and CO_2–Xe_2 trimers, *b* is again the symmetry axis, but the multiplicity of atomic isotopes means that spin statistics have less influence on the spectra.

II. RESULTS

The spectra were recorded as described previously,[9,19,28] using a rapid-scan optical parametric oscillator source to probe a pulsed supersonic slit jet expansion. The typical gas expansion mixture contained about 0.04% carbon dioxide plus 0.8% neon, argon, krypton, or xenon in helium carrier gas with a jet backing pressure of about 13 atm. Wavenumber calibration was carried out by simultaneously recording signals from a fixed etalon and a CO_2 reference gas cell. Simulation and fitting were carried out using PGOPHER software,[29] using the Mergeblend option to fit blended lines to an intensity weighted average of their components.

A. CO_2–Ne_2

Part of the observed spectrum showing CO_2–Ne_2 is illustrated in Fig. 2 (a broader view of the same spectrum is available in Fig. 1 of Ref. 9). Here, the strongest lines (and many of the weaker ones) belong to CO_2–Ne, CO_2–He, and $(CO_2)_2$. In spite of these many strong interfering lines, much of the relatively weak *Q*-branch of CO_2–Ne_2 (2349.3–2349.45 cm^{-1}) is fortunately clear of interference from other species, and many *P*- and *R*-branch transitions were also well resolved. This is a *c*-type perpendicular band (ΔK_a = ±1, ΔK_c = 0) with K_a = even levels in the ground state and K_a = odd in the excited state. The central *Q*-branch transitions noted in Fig. 2 have K_a = 1 ← 0, and we also assigned transitions with K_a = 5 ← 6, 3 ← 4, 1 ← 2, and 3 ← 2. Ultimately, 31 lines were assigned in terms of 34 transitions (there were a few blends) and fitted to obtain the parameters listed in Table I. The root mean square (rms) deviation was 0.000 21 cm^{-1}, approximately equal to our estimated experimental precision. Detailed line positions and assignments are given in the supplementary material. It was also possible to assign about 15 transitions to the mixed trimer CO_2–^{20}Ne–^{22}Ne (the natural abundance of ^{22}Ne is about 9%), with results as shown in Table I. For this species, there are of course no restrictions on the values of K_a. The rms deviation was 0.000 19 cm^{-1}.

B. CO_2–Ar_2

The lower panel of Fig. 3 shows the fundamental band of CO_2–Ar_2, previously studied by Sperhac *et al.*[21] This is a *c*-type band like that of CO_2–Ne_2, but now the symmetry axis is *b*, so as mentioned above the allowed levels in the lower state have (K_a, K_c) = (even, even) and (odd, odd). Note the relatively prominent *Q*-branch at 2348.24 cm^{-1}. The upper panel of Fig. 3 shows the new CO_2–Ar_2 combination band, which is a *b*-type band (ΔK_a = ±1, ΔK_c = ±1, ±3) with a noticeable gap in the center. This band looks complicated, but it was fairly easy to assign since we already had good ground state rotational parameters.[20,21] It has the advantage, compared to the fundamental, of being free from interference from stronger transitions due to other molecular species.

In order to analyze the spectra, we made a combined fit to the two present infrared bands and the appropriately weighted microwave data of Xu *et al.*,[20] with results as shown in Table II. A total of 52 lines were assigned in the fundamental and 105 in the combination band, and they were fitted with rms errors of 0.000 25 and 0.000 27 cm^{-1}, respectively. The 21 microwave transitions had an rms error of 1.3 kHz. Upper state centrifugal distortion

TABLE I. Molecular parameters for CO_2–Ne_2 (in cm^{-1}).[a]

	CO_2–$^{20}Ne_2$ ground state	CO_2–$^{20}Ne_2$ fundamental	CO_2–^{20}Ne–^{22}Ne ground state	CO_2–^{20}Ne–^{22}Ne fundamental
ν_0		2349.420 1(1)		2349.421 5(3)
A	0.112 244(37)	0.111 971(28)	0.108 665(70)	0.108 197(99)
B	0.080 417(28)	0.080 118(26)	0.078 629(29)	0.078 321(43)
C	0.060 634(64)	0.060 548(63)	0.058 54(18)	[0.058 45]
$10^5 \times \Delta_K$	2.51(31)	[2.51]	[2.51]	[2.51]
$10^5 \times \Delta_{JK}$	−1.66(39)	[−1.66]	[−1.66]	[−1.66]
$10^6 \times \Delta_J$	5.4(12)	[5.4]	[5.4]	[5.4]
$10^6 \times \delta_J$	−1.05(62)	[−1.05]	[−1.05]	[−1.05]

[a]Quantities in parentheses are 1σ from the least-squares fit, in units of the last quoted digit. Centrifugal distortion parameters were fixed to CO_2–$^{20}Ne_2$ ground state values as indicated by square brackets. For CO_2–^{20}Ne–^{22}Ne, $(C'-C'')$ was fixed to the CO_2–$^{20}Ne_2$ value.

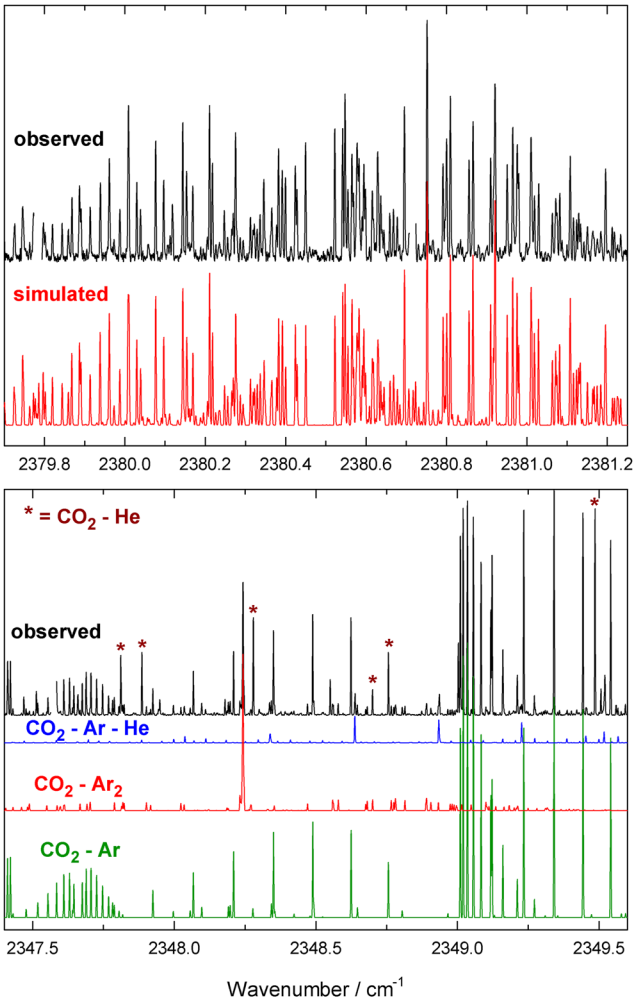

FIG. 3. Observed and simulated spectra showing the fundamental bands of CO_2–Ar_2 and CO_2–Ar–He (lower panel) and the combination band of CO_2–Ar_2 (upper panel).

parameters were constrained to ground state values for the fundamental but not for the combination band. The rationale for this was that the "vibrational environment" is similar for the ground and excited fundamental states but different for the combination state because of other nearby intermolecular modes, which affect the distortion parameters.

The earlier CO_2–Ar_2 studies[20,21] included sextic centrifugal distortion terms in their analyses, but we felt that the slight improvement of the fit was not worth the complication. Moreover, the earlier studies used a III^r representation, but CO_2–Ar_2 is not especially close to the oblate limit, and we found that a I^r representation (as used here) actually improves the fit (for example, by a factor of about 2.3 for the sum of squares in both 8 and 11 parameter fits to the microwave data[20]). This I^r vs III^r difference is probably not deeply meaningful, but the result encouraged us to stay with the more common I^r scheme. The switch to I^r from III^r explains the differences between our distortion parameters and the previous ones (e.g., the sign of δ_K).

Part of the observed spectrum of CO_2–Ar_2 in the region of the CO_2 $(01^11) \leftarrow (01^10)$ hot band is shown in Fig. 4. Its existence

TABLE II. Molecular parameters for CO_2–Ar_2 (in cm^{-1}).[a]

	Ground state	Fundamental	Combination
ν_0		2348.244 5(1)	2380.490 4(1)
A	0.059 000 938(21)	0.058 894 7(20)	0.056 783 7(67)
B	0.050 120 164(16)	0.050 072 1(26)	0.050 486 4(27)
C	0.031 241 461(12)	0.031 225 5(57)	0.030 740 6(12)
$10^7 \times \Delta_K$	7.769(11)	[7.769]	
$10^7 \times \Delta_{JK}$	−4.726(11)	[−4.726]	5.76(81)
$10^7 \times \Delta_J$	3.471 6(28)	[3.471 6]	
$10^7 \times \delta_K$	0.283 8(87)	[0.283 8]	
$10^7 \times \delta_J$	1.346 0(11)	[1.346 0]	

[a]Quantities in parentheses correspond to 1σ from the least-squares fit, in units of the last quoted digit. Fit includes ground state microwave data of Ref. 20. Ground and excited fundamental state centrifugal distortion parameters were constrained to be equal. This analysis uses a I^r representation, while those in Refs. 20 and 21 use a III^r representation.

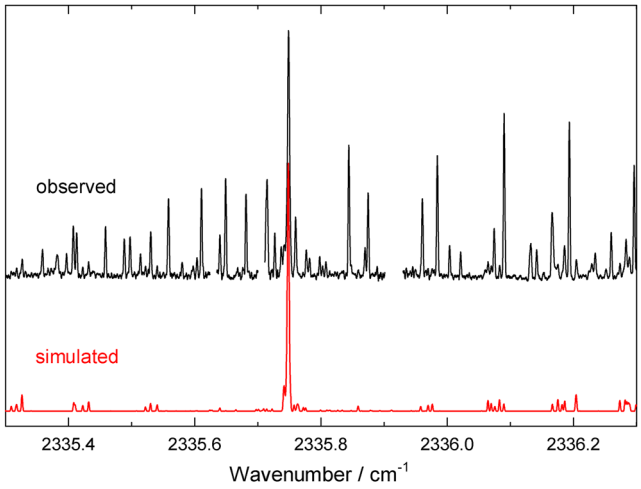

FIG. 4. Observed and simulated spectra of CO_2–Ar_2 in the region of the CO_2 (01^10) ← (01^10) hot band. Gaps in the observed spectrum correspond to regions of CO_2 monomer absorption. The simulated spectrum includes both the i-p and o-p modes. The many observed lines not in the simulation are due to CO_2–Ar.[15]

depends on the small fraction of CO_2 molecules which remain in the (01^10) vibrational state following supersonic expansion. As explained previously for the case of the dimer CO_2–Ar,[15] the presence of the nearby Ar atom(s) breaks the symmetry of the degenerate CO_2 (01^10) bending mode into in-plane (i-p) and out-of-plane (o-p) components. In the present case, the plane referred to is the symmetry plane containing CO_2 and bisecting the angle between the two Ar atoms. These i-p and o-p modes have A_1 and B_1 symmetry, respectively, for the lower (01^10) vibrational state and B_2 and A_2 symmetry for the upper (01^11) state. The hot band is *c*-type, the same as the fundamental, with (K_a, K_c) = (even, even) and (odd, odd) in the lower (01^10) vibrational state for the i-p mode and (K_a, K_c) = (even, odd) and (odd, even) for the o-p mode. From previous studies,[9,15,18,19] we expect strong Coriolis mixing (*c*-type in this case) between the i-p and o-p modes. The unresolved *Q*-branch of the CO_2–Ar_2 hot band at 2335.75 cm^{-1} is fairly strong, but the individual resolved *P*- and *R*-branch transitions are weak, as shown in Fig. 4. We assigned a total of 28 lines and fitted them with an rms error of 0.000 27 cm^{-1} to obtain the parameters listed in Table III. Due to the weakness of the spectrum and the relatively few assigned lines, it was prudent to highly constrain the fit. Thus, rotational constants were assumed to be the same for the i-p and o-p modes, changes in rotational constants between (01^10) and (01^11) were assumed to be the same as between (00^00) and (00^01) (i.e., the fundamental band, Table II), *C* was fixed at fundamental band values, and the Coriolis parameter, ξ_c, was assumed to equal to 2*C*. These are all reasonable approximations, based on the case of CO_2–Ar.[15] With these constraints, we obtained a value of 0.581(8) cm^{-1} for the separation between the i-p and o-p modes, with o-p lying above i-p. However, we feel that the real uncertainty in this value is significantly larger, based on our experience of trying different constraints in the fit. In the case of CO_2–Ar, the separation of 0.8773(2) cm^{-1} was determined to much higher precision and had the same sign.[15]

TABLE III. Molecular parameters for the (01^11) ← (01^10) hot band of CO_2–Ar_2 (in cm^{-1}).[a]

	(01^10)	(01^11)
σ_0 (i-p)	X[b]	2335.749 9(1) + X
σ_0 (o-p)	0.581(8) + σ_0 (i-p)	0.580(8) + σ_0 (i-p)
A	0.058 920(16)	[0.058 814]
B	0.050 142(20)	[0.050 094]
C	[0.031 241]	[0.031 225]
ξ_c	[0.062]	[0.062]

[a]Quantities in parentheses correspond to 1σ from the least-squares fit, in units of the last quoted digit. Quantities in square brackets were constrained at the indicated values (see text).
[b]X is equal to the free CO_2 ν_2 frequency (667.380 cm^{-1}) plus or minus a (small) unknown vibrational shift.

Is it possible to relate the splitting in the trimer to that in the dimer? If we denote the angle between the CO_2 bending plane and the CO_2–Ar dimer plane as ϕ, then (1) for $\phi = 0°$, the splitting of the CO_2 bending mode is the measured value of 0.877 cm^{-1}, (2) for $\phi = 45°$, the splitting must be zero, and (3) for $\phi = 90°$, it is −0.877 cm^{-1}. This dependence can be simply modeled as sinusoidal: (splitting) = 0.877 × cos(2ϕ). For the CO_2–Ar_2 trimer, the angle between each C–Ar bond and the symmetry plane bisecting the two bonds is $\phi = 33.2°$,[20] and the model would predict (splitting) = 2 × 0.877 × cos(66.4°) = 0.702 cm^{-1}. This does not agree particularly well with the measured value of 0.59 cm^{-1}, but the splitting dependence is not necessarily sinusoidal (reality could be more complicated), and, as mentioned, the experimental uncertainty is large.

C. CO_2–Kr_2

The fundamental and combination bands of CO_2–Kr_2 are illustrated in Fig. 5. The spectrum in the fundamental region is distinguished by a strong unresolved *Q*-branch feature at 2347.45 cm^{-1} surrounded by much weaker *P*- and *R*-branches, similar to CO_2–Ar_2 in Fig. 2 but with more structure. The added structure comes from the greater mass of CO_2–Kr_2 and also from the presence of more allowed rotational transitions due to the many trimers that contain unlike Kr isotopes and thus have all values allowed for (K_a, K_c). The weakness and complexity made assignment of the *c*-type fundamental band spectrum somewhat challenging; fortunately, it was possible to predict good preliminary rotational parameters in advance by assuming that the trimer structure was analogous to that of CO_2–Ar_2.

Interpretation of the combination band (upper panel of Fig. 5) posed further difficulties, in part because there is more Kr isotopic splitting here. To deal with this, we used a unified approach with scaled vibrational and rotational parameters to include all Kr isotopes, similar to the scheme developed previously for CO_2–Kr and CO_2–Xe.[18,19] The isotopic dependence of the rotational constants *A*, *B*, and *C* was first calculated for all combinations of the five most abundant Kr isotopes using a simple rigid model for the trimer structure. There are 15 such combinations with abundances ranging from 0.32 for CO_2–$^{84}Kr_2$ to 0.0005 for CO_2–$^{80}Kr_2$. Ten of these are unlike combinations with no spin statistics and

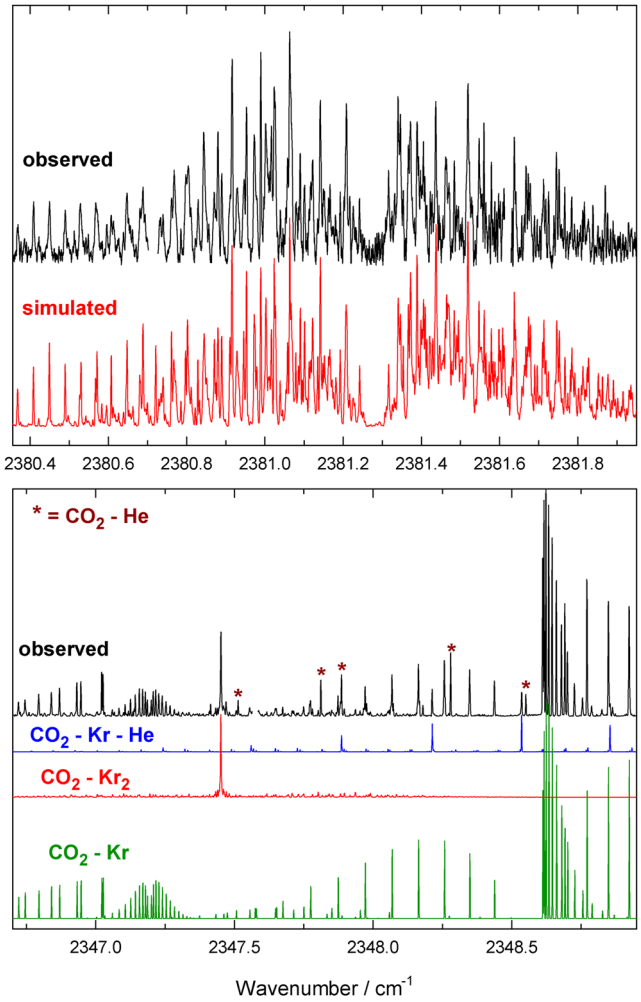

FIG. 5. Observed and simulated spectra showing the fundamental bands of CO_2–Kr_2 and CO_2–Kr–He (lower panel) and the combination band of CO_2–Kr_2 (upper panel). The simulations for CO_2–Kr_2 represent the sum of 15 isotopologues with scaled rotational and (for the combination band) vibrational parameters. Lines marked with an asterisk are due to CO_2–He.

a total abundance of 0.61, four are like combinations with statistical weights of 1:0 for levels with (K_a, K_c) = (ee, oo): (eo, oe) and a total abundance of 0.37, and one (CO_2–$^{83}Kr_2$) is a like combination with statistical weight 9:11 and an abundance of 0.013. The 15 isotopologues, their statistical abundances, and their rotational scaling factors are analogous to those described[18] for CO_2–Kr, and more details are given in the supplementary material. The same rotational scaling factors were used for all vibrational states. Previously for the dimers CO_2–Kr and –Xe, we introduced additional empirical fitting parameters to further refine the rotational isotope dependence, but this could not be done here because there are no precise microwave results available for CO_2–Kr_2 (unlike CO_2-Rg dimers and CO_2–Ar_2).

The isotope dependence of the combination band origin was modeled as

$$\nu_0(N_a, N_b) = \nu_0(N_0) + Offset \times ((N_a + N_b) - 2N_0),$$

where *Offset* is an adjustable parameter, N_a and N_b are the Kr atomic mass numbers of a particular isotopologue, and N_0 is the "standard" mass number, taken to be 84, the most abundant. Atomic mass *numbers* were used for convenience rather than the actual atomic masses. Of course, we know that vibrational frequencies do not scale linearly with Kr mass, rather (for example) as the square root of a reduced mass, but the difference is negligible here. Possible isotope dependence of the fundamental band origin seemed to be negligible here (it was previously found to be very small for CO_2–Kr and –Xe). It must be acknowledged that including 15 CO_2–Kr_2 isotopologues with abundances as low as 0.0005 in our fitting procedure amounted to overkill! However, it was actually fairly easy to do thanks to our previous experience with CO_2–Kr and –Xe and to the convenient features of the PGOPHER software, as highlighted in Ref. 19.

The unified fitting procedure just described greatly improved the fit and simulation of the combination band, as compared to fitting to a single "average" isotopologue, and it introduced only one additional variable (the *Offset* parameter). We also used the unified procedure for the fundamental (though it was less necessary) and analyzed both bands simultaneously. The results of this fit are listed in Table IV and shown by the simulations in Fig. 5. These parameters apply specifically to the "standard" species CO_2–$^{84}Kr_2$, and the scaled parameter values for the 14 other isotope combinations are given in the supplementary material. For the fundamental, 42 lines were fit with an rms error of 0.000 62 cm^{-1}, and for the combination band, 81 lines were fit with an error of 0.000 48 cm^{-1}. The *Offset* parameter in Table IV describes how much the combination band origin shifts with Kr atomic mass. Its value of −0.001 cm^{-1}/Dalton implies a total shift of the origin of only about 0.01 cm^{-1}, from 2381.290 cm^{-1} for CO_2–$^{80}Kr_2$ to 2381.276 cm^{-1} for CO_2–$^{86}Kr_2$.

In the CO_2 (01^11)–(01^10) hot band region, we observed a *Q*-branch due to CO_2–Kr_2 at 2334.948 cm^{-1} (it is visible in Fig. 3 of Ref. 18), analogous to that of CO_2–Ar_2 at 2335.750 cm^{-1} as described above. However, it was not possible to reliably assign enough *P*- and *R*-branch transitions to make a meaningful rotational analysis of the CO_2–Kr_2 hot band.

TABLE IV. Molecular parameters for CO_2–$^{84}Kr_2$ (in cm^{-1}).[a]

	Ground state	Fundamental	Combination
ν_0		2347.452 2(2)	2381.280 7(1)
A	0.047 285(10)	0.047 228(12)	0.045 208(13)
B	0.022 930(11)	0.022 916(11)	0.022 927(11)
C	0.016 683 5(65)	0.016 679 6(93)	0.016 523 9(66)
Offset			−0.001 14(15)

[a]Quantities in parentheses correspond to 1σ from the least-squares fit, in units of the last quoted digit. The parameter *Offset* expresses the Kr isotope dependence of the combination band origin and has effective units of cm^{-1}/Da.

D. CO_2–Xe_2

The fundamental and combination bands of CO_2–Xe_2 are illustrated in Fig. 6. The fundamental spectrum has a strong unresolved *Q*-branch feature at 2346.34 cm^{-1}. Line assignments in the weaker *P*- and *R*-branches were, like CO_2–Kr_2, challenging but still possible. The *b*-type combination band (upper panel of Fig. 6) has a central gap (like CO_2–Ar_2 and –Kr_2), considerable rotational structure in the *P*-branch region, and more blended structure in the *R*-branch.

To deal with Xe isotope effects, we used the unified scaled approach as described above for CO_2–Kr_2. This included the six most abundant Xe isotopes, giving a total of 21 isotopic combinations ranging in mass from CO_2–$^{129}Xe_2$ to CO_2–$^{136}Xe_2$. Fifteen of these are unlike combinations with no spin statistics and a total abundance of 0.75, five are like combinations with statistical weights

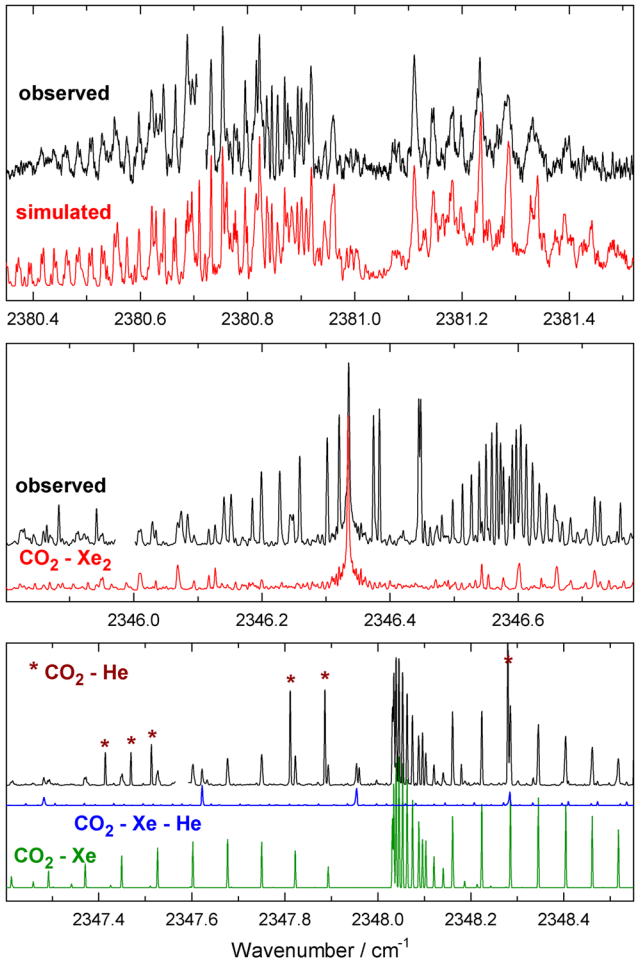

FIG. 6. Observed and simulated spectra showing the fundamental bands of CO_2–Xe_2 and CO_2–Xe–He (lower and middle panels) and the combination band of CO_2–Xe_2 (upper panel). The simulations for CO_2–Xe_2 represent the sum of 21 isotopologues with scaled rotational and (for the combination band) vibrational parameters. Observed lines in the CO_2–Xe_2 fundamental region (middle panel) not present in the simulation are due to CO_2–Xe.

TABLE V. Molecular parameters for CO_2–$^{131}Xe_2$ (in cm^{-1}).[a]

	Ground state	Fundamental	Combination
ν_0		2346.335 5(2)	2381.038 5(5)
A	0.041 232(12)	0.041 205(12)	0.040 601(24)
B	0.012 773(10)	0.012 779(11)	0.012 777(12)
C	0.010 244(12)	0.010 242(12)	0.010 183(14)
Offset			−0.000 78(20)

[a]Quantities in parentheses correspond to 1σ from the least-squares fit, in units of the last quoted digit. The parameter *Offset* expresses the Xe isotope dependence of the combination band origin and has effective units of cm^{-1}/Da.

of 1:0 for levels with (K_a, K_c) = (ee, oo): (eo, oe) and a total abundance of 0.16, and one (CO_2–$^{131}Xe_2$) is a like combination with statistical weight 3:5 and an abundance of 0.05. (Abundances do not quite total to 1 because ^{128}Xe was not included.) Further details are given in the supplementary material.

The unified fit was especially useful for the CO_2–Xe_2 combination band (top of Fig. 6), where it enabled us to achieve a rather good simulation that reproduces the dramatic difference between the *P*- and *R*-branch regions. The results of the fit are given in Table V. These parameters apply to CO_2–$^{131}Xe_2$, which was the "standard" species. Appropriately scaled values for the other isotopic species combinations are given in the supplementary material. For the fundamental, 44 lines were fit with an rms error of 0.000 43 cm^{-1}, and for the combination band, 31 lines were fit with an error of 0.000 48 cm^{-1}. The *Offset* parameter describing the shift of the combination band origin with Xe atomic mass has a value similar to that determined for CO_2–Kr_2. It represents a shift of the origin from 2381.042 cm^{-1} for CO_2–^{129}Xe to 2381.031 cm^{-1} for CO_2–^{136}Xe.

As in the case of CO_2–Kr_2, we observed a CO_2–Xe_2 *Q*-branch in the CO_2 (01^11)–(01^10) hot band region but could not assign further transitions sufficient for an analysis. The CO_2–Xe_2 *Q*-branch is located at 2333.811 cm^{-1}, and it may be seen in Fig. 4 of Ref. 19, located in among $K = 1 \leftarrow 2$ sub-band transitions of CO_2–Xe.

E. CO_2–Ne–He, CO_2–Ar–He, CO_2–Kr–He, and CO_2–Xe–He

Additional unexplained lines were observed in the fundamental band region that we eventually realized must be due to trimers containing CO_2 and the Rg atom being studied plus He. Their possible presence in the spectrum was not surprising since the supersonic expansion mixtures were predominantly composed of the helium carrier gas. Perhaps the most obvious of these new trimers was CO_2–Ne–He, which is the source of two noticeable lines located close to the *Q*-branch of CO_2–Ne_2. These lines, at 2349.272 and 2349.518 cm^{-1} (see Fig. 2), turn out to be unresolved *Q*-branches with $K_a = 0 \leftarrow 1$ and $1 \leftarrow 0$, respectively. Parts of the spectra due to CO_2–Ar–He, CO_2–Kr–He, and CO_2–Xe–He can be seen in Figs. 3, 5, and 6, respectively.

Continuing with CO_2–Ne–He as the example, we were able to assign about 18 lines, though some were very weak and perhaps a bit uncertain. In trying to assign and fit the lines, we faced a challenge: The light helium atom and its very weak interactions with CO_2 and Ne mean that we expect large-amplitude motions and significant centrifugal distortion effects. However, allowing many distortion

TABLE VI. Molecular parameters for CO_2-Rg-He trimers (in cm^{-1}).[a]

	CO_2–Ne–He *c*-type	CO_2–Ar–He (*c*-type)	CO_2–Kr–He *c*-type	CO_2–Xe–He *c*-type
ν_0	2349.397 5(4)	2348.787 7(4)	2348.375 0(5)	2347.788 9(2)
A'	0.210 51(16)	0.203 92(10)	0.200 44(10)	0.197 344(61)
A''	0.214 90(18)	0.205 64(12)	0.202 26(14)	0.199 258(74)
$(B + C)/2$	0.089 301(61)	0.056 473(45)	0.039 68(11)	0.031 440(25)
$(B - C)$	0.000 42(9)	0.000 01(6)	0.000 05(12)	0.000 111(31)
n	18	33	13	32
rmsd	0.001 0	0.001 3	0.000 8	0.000 8

[a]Quantities in parentheses are 1σ from the least-squares fit, in units of the last quoted digit. n is the number of assigned lines (some of which are blends of multiple transitions), and rmsd is the root mean square error of the fit.

parameters to vary in both the ground and excited states might be dangerous, considering the limited number of assigned lines.

There is a further complication: the possibility of He atom tunneling. In the case of CO_2–He_2,[22] there is significant tunneling involving motion of the He atoms around the "equator" of the CO_2 through a transition state with a linear He–C–He configuration. The tunneling barrier is not large since the He–He attraction is weak and the He mass is small. The result is a relatively large tunneling splitting, calculated to be about 0.50 cm^{-1} for CO_2–He_2.[22] Rotational levels of the ground tunneling state ($v_t = 0$) have even values of K_a'', while those of the first excited tunneling state ($v_t = 1$, at 0.5 cm^{-1}) have odd values of K_a''. The two tunneling states have significantly different rotational constants (since their vibrational wave functions are different), for example, $A \approx 0.30$ cm^{-1} for $v_t = 0$ and $A \approx 0.21$ cm^{-1} for $v_t = 1$, so that different rotational constants are needed for even and odd K_a'' transitions.[22] Of course for the present case of CO_2–Ne–He, the tunneling barrier will certainly be larger. However, the possibility of needing different rotational constants for K_a'' = even and odd transitions further challenged our assignment and fitting of the spectrum.

We tried including various centrifugal distortion parameters as well as separately fitting K_a'' = even and odd transitions for CO_2–Ne–He and the other mixed trimers. Of course, the fits improved as more parameters were varied, but at the same time our confidence in the results diminished! So in the end, we decided to use highly constrained fits with few parameters, and these are the results given in Table VI. The values of $(B + C)/2$ and $(B - C)$ were constrained to be equal in the ground and upper vibrational states, while A was allowed to vary separately in the two states. The constraint is not unreasonable, as demonstrated in Tables I and III–V. Interestingly, all the CO_2-Rg-He trimers turn out to be (accidental) near-symmetric rotors. In all cases, the observed transitions appeared to be *c*-type. However, since the values of $(B - C)$ were very small (insignificant for CO_2–Ar–He and CO_2–Kr–He), the distinction between *b*- and *c*-type transitions is not very meaningful.

III. DISCUSSION

A. Combination bands

The combination bands observed here result in intermolecular mode frequency values for CO_2–Ar_2, –Kr_2, and –Xe_2 as given in Table VII, where they are compared to the previously measured intermolecular bending frequencies of the corresponding CO_2-Rg dimers. (When we say "intermolecular," each Rg atom is considered to be a "molecule.") Note that the trimer frequencies are consistently about 15% larger than the dimer ones. The trimer combination bands were observed to have *b*-type rotational selection rules, which tells us that the combination mode has A_1 symmetry (in the C_{2v} point group appropriate for trimers with indistinguishable Rg atoms). Since the intramolecular fundamental (CO_2 ν_3) is B_1, this means that the intermolecular mode must also be B_1 in order to get the A_1 combination band ($B_1 \otimes B_1 = A_1$).

CO_2-Rg_2 trimers have five intermolecular vibrational modes, described as follows:

1. Rg_2-CO_2 van der Waals stretch (A_1 symmetry);
2. Rg-Rg van der Waals stretch (A_1);
3. torsion, or asymmetric Rg-C–O bend (A_2);
4. CO_2 rock, or "Rg_2 flap,"[20] or symmetric Rg-C-O bend (B_1);
5. Rg_2 rock, or asymmetric Rg-C stretch (B_2).

In Ref. 20, these modes correspond to coordinates S_3, S_4, S_5, S_7, and S_9, and in Ref. 21 they correspond to R, ρ, θ_x, θ_y, and χ, respectively. There is only one possible B_1 mode, so it is evident that our observed combination bands must involve the CO_2 rocking motion. This is not surprising since the trimer rocking mode is analogous to the CO_2-Rg dimer bending mode, and they have similar values as noted above. Arguments based on C_{2v} symmetry do not strictly apply to trimers with inequivalent Rg atoms, in which case the torsional mode could in principle also cause the observed combination bands. However, there can be no

TABLE VII. Comparison of observed intermolecular bending frequencies for CO_2-Rg_2 trimers and CO_2-Rg dimers (in cm^{-1}).

Rg	CO_2-Rg_2	CO_2-Rg[a]
Ne		17.716
Ar	32.246	27.818
Kr	33.829	29.429
Xe	34.703	30.574

[a]From Refs. 9, 12, 18, and 19, respectively.

TABLE VIII. Vibrational frequency shifts in CO_2-Rg dimers and CO_2-Rg_2 trimers (in cm^{-1}).

Rg	CO_2-Rg minus CO_2	CO_2-Rg_2 minus CO_2-Rg	Difference	CO_2-Rg-He minus CO_2-Rg
Ne	+0.1364	+0.1405	+0.0041	+0.1179
Ar	−0.4706	−0.4281	+0.0425	+0.1151
Kr	−0.8847	−0.8063	+0.0784	+0.1165
Xe	−1.4719	−1.3358	+0.1361	+0.1176

doubt that that the CO_2 rock remains the real assignment. In the case of CO_2–Ne_2, a combination band has not yet been observed. Since the CO_2–Ne_2 *a*- and *b*-inertial axes are interchanged relative to the other trimers, we expect its analogous combination band to be *a*-type.

B. Vibrational shifts

Vibrational shifts observed for CO_2-Rg_2 trimers relate directly to the interesting question of non-additive intermolecular effects, as was carefully analyzed in the CO_2–Ar_2 paper of Sperhac *et al.*[21] The present results are listed in Table VIII, where the first column gives the Rg atom, the second column gives (previously known) shifts for CO_2-Rg dimers relative to the free CO_2 molecule, and the third column gives the additional shift induced by adding the second Rg atom to form a trimer.

The shifts in columns two and three are similar as expected since each Rg atom in a trimer occupies a position equivalent (relative to CO_2) to the position of the Rg atom in the dimer. The notable trend in Table VIII is that the incremental shifts in column three are always more positive (i.e., blue-shifted) compared to column two. This deviation from linearity (column three minus column two) is shown in column four of Table VIII, and it is especially significant since it is precisely (≈0.0002 cm^{-1}) determined and has a clear meaning. Sperhac *et al.*[21] argued that this quantity (in their case, the difference between the incremental shifts in CO_2–Ar and CO_2–Ar_2) is an essentially exact measure of differential three-body effects (i.e., the *change* in three-body effects between the CO_2 ground state and excited ν_3 state). Their model calculation suggested that most of this effect was due to competing induced dipole–induced dipole and exchange quadrupole terms. However, their quantitative agreement with experiment was not very good, and the need to integrate over the CO_2 ν_3 motion was emphasized. When this was done in a subsequent *ab initio* calculation by Rak *et al.*,[30] much better agreement with experiment was indeed achieved. However, the authors pointed out that the agreement might have been fortuitous "in view of the fact that the effects of intermolecular vibrations were not included." In addition to these effects of zero-point intermolecular motion, the effects of the other intramolecular (CO_2) modes could also be significant, as shown for ν_1 in the case of CO_2–He.[31,32] In any case, the new results reported here for CO_2–Ne_2, –Kr_2, and –Xe_2 provide further direct and straightforward tests for these calculations.

The final column of Table VIII shows the incremental vibrational shift resulting from addition of a helium atom to a CO_2-Rg dimer to form a CO_2-Rg-He trimer, and we see that the shift is almost the same (≈+0.117 cm^{-1}) for all the mixed trimers. This value is somewhat greater than the shift of +0.095 cm^{-1} reported by Weida *et al.* for CO_2–He relative to CO_2 itself. However, in a reanalysis (unpublished), we obtain a more similar shift of +0.116 cm^{-1} for $^{12}C^{16}O_2$–He (see also Ref. 4 for other CO_2 isotopologues of CO_2–He).

C. Structures

Determining precise geometrical structures for weakly bound molecular complexes can be a frustrating or even meaningless task because of their large-amplitude intermolecular motions, but of course we still like to try! Given the C_{2v} symmetry of the CO_2-Rg_2 trimers, only two parameters are required to specify an equilibrium structure: the Rg-Rg distance, r(Rg-Rg), and the C-Rg distance, r(C-Rg). Alternately, one can use the CO_2 to Rg_2 center of mass distance, $R_{c.m.}$, since $r(\text{C-Rg})^2 = R_{c.m.}^2 + (r(\text{Rg-Rg})/2)^2$. The trimer structures are thus overdetermined since it is not possible to exactly match three rotational parameters by varying two structural parameters. In Table IX, we show the results of two-parameter

TABLE IX. Comparison of structural parameters in CO_2-Rg_2, CO_2-Rg, and Rg_2 (lengths in Å, angles in degrees).

	CO_2-Rg_2 r_0(C-Rg)	CO_2-Rg_2 r_0(Rg-Rg)	CO_2-Rg_2 r_0(C-Rg)	CO_2-Rg_2 r_0(Rg-Rg)	CO_2-Rg_2 θ_y[a]			
Rg	2 parameter		3 parameter			CO_2-Rg r_0(C-Rg)[b]	Rg_2 r_0(Rg-Rg)	Rg_2 r_e(Rg-Rg)[c]
Ne	3.276	3.295	3.268	3.307	11.5	3.290	3.337[d]	3.084
Ar	3.504	3.839	3.499	3.843	11.2	3.504	3.827[e]	3.755
Kr	3.629	4.066	3.623	4.069	13.2	3.624	4.059[f]	4.012
Xe	3.828	4.436	3.823	4.437	12.3	3.815		4.375

[a]Deviation from 90° of the angle ($Rg_{2c.m.}$-C-O); $Rg_{2c.m.}$ = Rg_2 center of mass.
[b]Experimental r_0 values from the work of Randall, Walsh, and Howard.[5]
[c]Theoretical r_e from the work of Deiters and Sadus.[34]
[d]Experimental r_0 for Ne_2 from the work of Wüest and Merkt.[35]
[e]Experimental r_0 for Ar_2 from the work of Mizuse *et al.*[36]
[f]Experimental r_0 for Kr_2 from the work of LaRocque *et al.*[37]

least-squares fits to obtain r(Rg-Rg) and r(C-Rg), made using the simple and effective strfit and pmifst programs of Kisiel.[33] As expected, the present structural parameters for CO_2–Ar_2 are very similar to those of Refs. 20 and 21.

To extend their two-parameter CO_2–Ar_2 fit, Sperhac *et al.*[21] proceeded to make an effective three-parameter fit by varying the parameter χ in addition to r(Rg-Rg) and r(C-Rg). χ is the angle describing the intermolecular Rg_2 rocking mode, or, more precisely, the deviation from 90° of the angle subtended by an Ar atom, the Ar_2 center of mass, and the C atom. However, we think the description[21] of their three-parameter fit must be incorrect. It is clear from their Table III that varying χ affects only the P_x and P_y planar moments. P_x is also sensitive to r(Rg-Rg) and P_y to r(C-Rg). Thus χ cannot improve the result already achieved in a two-parameter fit, since P_z is not influenced by r(Rg-Rg), r(C-Rg), or χ. Rather, it is necessary to vary one of the remaining structural parameters: θ_x (which we call torsion above) or θ_y (which we call CO_2 rock). It appears that Sperhac *et al.* actually varied θ_y in their three-parameter fit, and this is also what we have varied for our three-parameter fits (Table IX). Our θ_y value of 11.2° for CO_2–Ar_2 is almost the same as the 11.4° value reported by Sperhac *et al.*, which they labeled as χ.

The angle θ_y is a logical choice for the third parameter, since it is similar to the angle θ varied in two-parameter fits of CO_2-Rg dimers.[5] We see in Table IX that θ_y has fairly similar values (11.2°–13.2°) for all four CO_2-Rg_2 trimers and that r(Rg-Rg) and r(C-Rg) do not change very much between the two- and three-parameter fits. In the case of the CO_2-Rg dimers, θ has values of 6.6°–8.6°.[5] However, in a trimer, θ (deviation from 90° of angle Rg-C-O) and θ_y (deviation from 90° of angle $Rg_{2c.m.}$-C–O) are not quite the same geometrically, with θ necessarily being smaller than θ_y. So, the actual trimer θ-values range from about 9° to 11°, which is really quite similar to the dimer values. Of course, these effective angles do not correspond to equilibrium structures (where θ and θ_y equal zero). Rather, they provide measures of the rms value of the particular coordinate averaged over its zero-point wavefunction. For CO_2-Rg dimers, with just two intermolecular coordinates, the effective values of R and θ are relatively meaningful and easy to interpret. For CO_2-Rg_2 trimers with five intermolecular coordinates, the meaning of a three-parameter fit is not so clear since the effects of the remaining two coordinates have necessarily been ignored.

The r(C-Rg) bond length values for CO_2-Rg_2 trimers in Table IX are very similar to the corresponding CO_2-Rg dimer values, as expected. For a comparison of Rg-Rg bond lengths, we have experimental r_0(Rg-Rg) (zero-point average) values from rotationally resolved spectra of Ne_2, Ar_2, and Kr_2, and these compare quite well with our CO_2-Rg_2 trimer results. Rotationally resolved Xe_2 spectra are not available, so we only have theoretical r_e(Rg-Rg) (equilibrium) values for comparison, and these of course are systematically smaller than the CO_2-Rg_2 trimer r_0(Rg-Rg) results.

IV. CONCLUSIONS

We have studied high-resolution spectra of CO_2-Rg_2 trimers (Rg = Ne, Ar, Kr, Xe) as observed in the CO_2 ν_3 fundamental band region (≈2350 cm^{-1}), thus extending previous work on CO_2–Ar_2.[20,21] The precisely measured vibrational frequency shifts and intermolecular CO_2 rocking mode frequencies provide sensitive new tests for intermolecular potential energy calculations. When compared to the vibrational shifts in the CO_2-Rg clusters, the measured vibrational shifts in the CO_2-Rg_2 clusters provide precise and straightforward measure of nonadditive three-body effects. Moreover, the reported rotational constants should aid in the possible detection of pure rotational microwave spectra for Rg = Ne, Kr, and Xe, though the latter two will be complicated by the possibility of many isotopic species. We are continuing to analyze the spectra of larger CO_2-Rg_n clusters and have recently reported the observation of highly symmetric structures for CO_2–Ar_{15} and CO_2–Ar_{17}, with the latter marking the completion of the first solvation shell for CO_2 in Ar.[38]

SUPPLEMENTARY MATERIAL

The supplementary material includes tables giving the observed and fitted line positions for CO_2-Rg_2 trimers and isotope specific parameters for CO_2–Kr_2 and CO_2–Xe_2.

ACKNOWLEDGMENTS

The financial support of the Natural Sciences and Engineering Research Council of Canada is gratefully acknowledged.

AUTHOR DECLARATIONS

Conflict of Interest

The authors have no conflicts to disclose.

Author Contributions

A. J. Barclay: Data curation (equal); Investigation (equal); Validation (equal). **A. R. W. McKellar**: Formal analysis (equal); Validation (equal); Writing – original draft (equal); Writing – review & editing (equal). **N. Moazzen-Ahmadi**: Conceptualization (equal); Funding acquisition (equal); Project administration (equal); Supervision (equal); Validation (equal); Writing – review & editing (equal).

DATA AVAILABILITY

The data that support the findings of this study are available within the article and its supplementary material.

REFERENCES

[1] J. M. Steed, T. A. Dixon, and W. Klemperer, "Determination of the structure of $ArCO_2$ by radio frequency and microwave spectroscopy," J. Chem. Phys. **70**, 4095–4100 (1979); Erratum **75**, 5977 (1981).

[2] M. J. Weida, J. M. Sperhac, D. J. Nesbitt, and J. M. Hutson, "Signatures of large amplitude motion in a weakly bound complex: High-resolution IR spectroscopy and quantum calculations for $HeCO_2$," J. Chem. Phys. **101**, 8351 (1994).

[3] Y. Xu and W. Jäger, "Fourier transform microwave spectra of the very weakly bound He–CO_2 dimer," J. Mol. Struct. **599**, 211 (2001).

[4]A. R. W. McKellar, "Infrared spectra of isotopic CO_2–He complexes," J. Chem. Phys. **125**, 114310 (2006).
[5]R. W. Randall, M. A. Walsh, and B. J. Howard, "Infrared absorption spectroscopy of rare-gas–CO_2 clusters produced in supersonic expansions," Faraday Discuss. Chem. Soc. **85**, 13–21 (1988).
[6]G. T. Fraser, A. S. Pine, and R. D. Suenram, "Optothermal-infrared and pulsed-nozzle Fourier-transform microwave spectroscopy of rare gas–CO_2 complexes," J. Chem. Phys. **88**, 6157–6167 (1988).
[7]Y. Xu and W. Jäger, "Rotational spectra of $NeCO_2$ isotopomers," J. Mol. Spectrosc. **192**, 435–440 (1998).
[8]T. Konno, S.-i. Fukuda, and Y. Ozaki, "Infrared spectroscopy of Ne–$^{12}C^{18}O_2$ and Xe–$^{12}C^{18}O_2$: Change in the CO_2 intramolecular potential by formation of rare gas–CO_2 complexes," Chem. Phys. Lett. **421**, 421–426 (2006).
[9]A. J. Barclay, A. R. W. McKellar, and N. Moazzen-Ahmadi, "New infrared spectra of CO_2–Ne: Fundamental for CO_2–^{22}Ne isotopologue, intermolecular bend, and symmetry breaking of the intramolecular CO_2 bend," Chem. Phys. Lett. **779**, 138874 (2021).
[10]H. Mäder, N. Heineking, W. Stahl, W. Jäger, and Y. Xu, "Rotational spectrum of the isotopically substituted van der Waals complex Ar–CO_2 investigated with a molecular beam Fourier transform microwave spectrometer," J. Chem. Soc., Faraday Trans. **92**, 901–905 (1996).
[11]S. W. Sharpe, R. Sheeks, C. Wittig, and R. A. Beaudet, "Infrared absorption spectroscopy of CO_2-Ar complexes," Chem. Phys. Lett. **151**, 267–272 (1988).
[12]S. W. Sharpe, D. Reifschneider, C. Wittig, and R. A. Beaudet, "Infrared absorption spectroscopy of the CO_2–Ar complex in the 2376 cm^{-1} combination band region: The intermolecular bend," J. Chem. Phys. **94**, 233–238 (1991).
[13]Y. Ozaki, K. Horiai, T. Konno, and H. Uehara, "Infrared absorption spectroscopy of Ar–$^{12}C^{18}O_2$: Change in the intramolecular potential upon complex formation," Chem. Phys. Lett. **335**, 188–194 (2001).
[14]J. Thiévin, Y. Cadudal, R. Georges, and A. A. Vigasin, "Direct FTIR high resolution probe of small and medium size $Ar_n(CO_2)_m$ van der Waals complexes formed in a slit supersonic expansion," J. Mol. Spectrosc. **240**, 141–152 (2006).
[15]T. A. Gartner, A. J. Barclay, A. R. W. McKellar, and N. Moazzen-Ahmadi, "Symmetry breaking of the bending mode of CO_2 in the presence of Ar," Phys. Chem. Chem. Phys. **22**, 21488 (2020).
[16]M. Iida, Y. Ohshima, and Y. Endo, "Induced dipole moments and intermolecular force fields of rare gas-CO_2 complexes studied by Fourier-transform microwave spectroscopy," J. Phys. Chem. **97**, 357–362 (1993).
[17]T. Konno, S.-i. Fukuda, and Y. Ozaki, "Infrared spectroscopy of Kr–$^{12}C^{18}O_2$: Change in the CO_2 intramolecular potential by complex formation and isotope effect on the vibrationally averaged intermolecular geometry," Chem. Phys. Lett. **414**, 331–335 (2005).
[18]T. Gartner, S. Ghebretnsae, A. R. W. McKellar, and N. Moazzen-Ahmadi, "Spectra of CO_2–Kr in the 4.3 μm region: Intermolecular bend and symmetry breaking of the intramolecular CO_2 bend," ChemistrySelect **7**, e202202601 (2022).
[19]A. J. Barclay, A. R. W. McKellar, C. M. Western, and N. Moazzen-Ahmadi, "New infrared spectra of CO_2–Xe: Modelling Xe isotope effects, intermolecular bend and stretch, and symmetry breaking of the CO_2 bend," Mol. Phys. **119**, e1919325 (2021).
[20]Y. J. Xu, W. Jager, and M. C. L. Gerry, "Pulsed molecular beam microwave Fourier transform spectroscopy of the van der Waals trimer Ar_2-CO_2," J. Mol. Spectrosc. **157**, 132 (1993).
[21]J. M. Sperhac, M. J. Weida, and D. J. Nesbitt, "Infrared spectroscopy of Ar_2CO_2 trimer: Vibrationally averaged structures, solvent shifts, and three-body effects," J. Chem. Phys. **104**, 2202 (1996).
[22]J. Tang, A. R. W. McKellar, X.-G. Wang, and T. Carrington, Jr., "Theoretical and experimental study of infrared spectra of He_2-CO_2," Can. J. Phys. **87**, 417–423 (2009).
[23]M. Rezaei, K. H. Michaelian, A. R. W. McKellar, and N. Moazzen-Ahmadi, "Infrared spectra of the Ne_2–N_2O, Ar_2–N_2O trimers," J. Mol. Spectrosc. **278**, 17–22 (2012).
[24]Y. Xu, M. C. L. Gerry, J. P. Connelly, and B. J. Howard, "The microwave spectrum, structure, and harmonic force field of the van der Waals trimer Ar_2–OCS," J. Chem. Phys. **98**, 2735 (1993).
[25]Y. Xu and W. Jäger, "Spectroscopic investigation of the ternary Ne–Ne–OCS van der Waals cluster: Additive and non-additive interactions," Phys. Chem. Chem. Phys. **2**, 3549 (2000).
[26]H. S. Gutowsky, T. D. Klots, and C. E. Dykstra, "Rotational spectrum and potential surface for Ar_2–HCN: A T-shaped cluster with internal rotation," J. Chem. Phys. **93**, 6216 (1990).
[27]Z. Kisiel, B. A. Pietrewicz, and L. Pszczółkowski, "The observation and characterization by rotational spectroscopy of the weakly bound trimer Ar_2HBr," J. Chem. Phys. **117**, 8248 (2002).
[28]M. Rezaei, S. Sheybani-Deloui, N. Moazzen-Ahmadi, K. H. Michaelian, and A. R. W. McKellar, "CO dimer: The infrared spectrum revisited," J. Phys. Chem. A **117**, 9612–9620 (2013).
[29]C. M. Western, J. Quant. Spectrosc. Radiat. Transfer **186**, 221 (2017).
[30]J. Rak, M. M. Szczęśniak, G. Chałasiński, and S. M. Cybulski, "The effect of two- and three-body interactions in Ar_n CO_2 (n=1,2) on the asymmetric stretching CO_2 coordinate: An *ab initio* study," J. Chem. Phys. **106**, 10215 (1997).
[31]H. Li and R. J. Le Roy, "Analytic three-dimensional 'MLR' potential energy surface for CO_2–He, and its predicted microwave and infrared spectra," Phys. Chem. Chem. Phys. **10**, 4128–4137 (2008).
[32]H. Li, N. Blinov, P.-N. Roy, and R. J. Le Roy, "Path-integral Monte Carlo simulation of ν_3 vibrational shifts for CO_2 in $(He)_n$ clusters critically tests the He–CO_2 potential energy surface," J. Chem. Phys. **130**, 144305 (2009).
[33]Z. Kisiel, PROSPE—Programs for Rotational Spectroscopy, http://info.ifpan.edu.pl/~kisiel/prospe.html.
[34]U. K. Deiters and R. J. Sadus, "Two-body interatomic potentials for He, Ne, Ar, Kr, and Xe from *ab initio* data," J. Chem. Phys. **150**, 134504 (2019).
[35]A. Wüest and F. Merkt, "Determination of the interaction potential of the ground electronic state of Ne_2 by high-resolution vacuum ultraviolet laser spectroscopy," J. Chem. Phys. **118**, 8807 (2003).
[36]K. Mizuse, U. Sato, Y. Tobata, and Y. Ohshima, "Rotational spectroscopy of the argon dimer by time-resolved Coulomb explosion imaging of rotational wave packets," Phys. Chem. Chem. Phys. **24**, 11014–11022 (2022).
[37]P. E. LaRocque, R. H. Lipson, P. R. Herman, and B. P. Stoicheff, "Vacuum ultraviolet laser spectroscopy. IV. Spectra of Kr_2 and constants of the ground and excited states," J. Chem. Phys. **84**, 6627 (1986).
[38]A. J. Barclay, A. R. W. McKellar, and N. Moazzen-Ahmadi, "Observing the completion of the first solvation shell of carbon dioxide in argon from rotationally resolved spectra," J. Phys. Chem. Lett. **13**, 6311–6315 (2022).